Scientific Visualization, 2025, volume 17, number 5, pages 72 - 82, DOI: 10.26583/sv.17.5.08

Determination of Adiabatic Wall Temperature in High-Speed Gas Flows Using Infrared Thermography

N.S. Malastowski[1], N.A. Kiselev[2], A.G. Zditovets[3], Y.A. Vinogradov[4]

Lomonosov Moscow State University, Institute of Mechanics, Moscow, Russia

[1] ORCID: 0000-0002-1285-1748, nik_malans@mail.ru
[2] ORCID: 0009-0009-5552-5457, kiselev.nick.a@yandex.ru
[3] ORCID: 0000-0002-4532-1014, zditovets@mail.ru
[4] ORCID: 0009-0004-8647-0405, vinograd@imec.msu.ru

Abstract

This paper presents a method for the non-contact determination of the adiabatic wall temperature in high-speed gas flows. The method is based on the processing of a sequence of thermograms obtained using an IR camera, within a program developed in Python 3.10. The approach demonstrated high efficiency when handling large datasets, particularly concerning minimizing temporal and computational demands. The adiabatic wall temperature was determined under both steady-state conditions, directly in the experiment, and transient conditions, through the extrapolation of the heat flux as a function of the current temperature of the examined surface. The effectiveness of this method was demonstrated in the investigation of non-mechanical energy separation in compressible gas flows.

Keywords: high-speed flows, heat transfer, boundary layer, adiabatic wall temperature, thermometry, non-contact methods.

1. Introduction

The improvement of experimental methods for investigating heat transfer in high-speed gas flows remains a topic of ongoing importance. This is largely due to the significant challenges associated with probe-based measurements in high-speed gas flows primarily arising from the small physical thickness of the boundary layers. As a result, many experimental studies are limited to low-speed flows, where velocities rarely exceed 10 m/s [1]. Based on the similarity of the processes governing boundary layer formation, results obtained under these conditions are often extrapolated to high-speed flows, with corrections for compressibility, non-isothermal effects, and other factors. Consequently, there has been a growing interest in non-contact methods for determining key quantities that govern heat transfer at fluid-solid interfaces, such as heat fluxes, heat transfer coefficients, and the temperatures of thermally insulated (adiabatic) walls [2].

Such methods include infrared thermography, which allows the recording of surface temperatures of objects in gas flows. Like other experimental techniques, infrared thermography is of particular importance in the validation of mathematical models integrated into industrial software [3]. However, unlike classical image processing tasks applied in thermophysics and fluid mechanics—such as the analysis of bubble evolution laws in liquid flows [4–6] or the tracking of disturbances, including shock waves and other inhomogeneities [7,8]— the temperature values at each point in a thermogram are related to each other through the governing equation of heat conduction. This relationship provides additional opportunities for the study of thermal regimes in technical systems [9] and for evaluating the influence of heat transfer on the parameters of gas flows [10].

An image captured by a thermographic camera represents a self-contained dataset, often not requiring the use of specialized methods typically associated with computer vision systems [11]. The primary task in this context is the interpretation and subsequent application of the obtained images to establish correlations between the physical processes governing the temperature field of the investigated objects.

At the gas-solid interface, the most effective method for describing heat transfer is the specification of the third type boundary condition (Robin boundary condition)—namely, the heat transfer coefficient and the adiabatic wall temperature. The determination of the adiabatic wall temperature is also crucial for accurately describing the effects of compressibility and non-isothermal conditions in the boundary layers of high-speed gas flows. As demonstrated in [12], the stagnation temperature of the flow can vary across the boundary layer thickness when a flat thermally insulated plate is subjected to the flow. Consequently, the temperature of the gas in direct contact with the surface of the thermally insulated body will differ from that of the core flow. This temperature is usually called the adiabatic wall temperature (T_{aw}), and in the simplest case of flow over a flat plate depends on the stagnation temperature, Mach number, Reynolds number, and Prandtl number. In engineering applications, it is typically expressed as follows:

$$T_{aw} = T_0 \frac{1 + r\frac{k-1}{2}M^2}{1 + \frac{k-1}{2}M^2} \quad (1)$$

where r is the temperature recovery factor, T_o, and M are the stagnation temperature, and the Mach number of the free flow respectively, while k is the specific heat ratio of the gas. Experimental data [13,14] indicate that the temperature recovery factor for a flat plate is largely independent of the Mach and Reynolds numbers. For fully developed laminar and turbulent air flows, their values are approximately 0.85 ± 0.01 and 0.89 ± 0.01, respectively. In the processing of experimental data for turbulent flows, the recovery factor is typically assumed to lie within the range of r = 0.89 to 1.0, whereas for laminar flows, it is generally taken as 0.85 [15–22]. However, for more complex flow regimes, the recovery factor may deviate substantially from these values, often requiring its experimental determination.

Accurate determination of the adiabatic wall temperature is crucial for evaluating the efficiency of thermal separation in non-mechanical energy separation devices [23]. The operational principle of these devices relies on the difference between the adiabatic wall temperature T_{aw} and the stagnation temperature of the flow, as well as the dependence of this temperature difference on the Mach number M of the incoming flow [24] and other external conditions. It is evident that flows, separated by a thermally conductive wall and having identical stagnation temperatures but differing adiabatic wall temperatures, will engage in heat transfer. From a design standpoint, the experimental determination of the adiabatic wall temperature represents a critical practical challenge, which can be effectively addressed using thermographic imaging.

The adiabatic wall temperature can be directly derived from thermograms of thermally insulated objects under controlled laboratory conditions. However, in experiments, it is far more common that thermal insulation of the object under study cannot be achieved. In such cases, the data processing procedure involves reconstructing the heat fluxes to analyze heat transfer conditions for flow regimes in which a difference exists between the adiabatic and measured wall temperatures [25–28]. Various algorithms can be applied to these tasks, taking into account factors such as the high thermal conductivity of the channel wall material [25], extreme flow conditions with Mach numbers up to approximately 7.5 [26], and the complex geometric configuration of the object under study [27,28].

In conclusion, developing and improving methodologies for extracting information from thermogram sequences obtained during thermophysical experiments remains a significant practical challenge aimed at advancing the understanding of heat transfer phenomena in high-speed gas flows.

2. Methodology

This paper presents two investigations aimed to determine the adiabatic wall temperature in a compressible air flow. The first study examines quasi-stationary temperature fields of thermally insulated objects (circular cylinders). In contrast, the second study, where thermal insulation of the object could not be achieved, requires recording of the unsteady temperature field of the cooled surface of a supersonic channel to determine the adiabatic wall temperature. As previously noted, for thermally insulated objects, under prolonged exposure and the achievement of a quasi-steady state, the surface temperature becomes equal to the adiabatic wall temperature. However, accurately determining the adiabatic wall temperature under heat transfer conditions between the wall and the gas requires extrapolation of the dependence of heat flux on wall temperature [2].

In both cases, detailed information regarding the adiabatic wall temperature fields was obtained by recording the temperature distributions of the investigated surfaces using the INFRATEC 8800 infrared camera. In the first study, quasi-steady flow regimes were measured at a frame rate of 0.2 Hz, while in the second study, the frame rate was 30 Hz. The spatial resolution of the images was approximately 2 pixels per millimeter.

Data acquisition and initial thermogram processing were performed using the "IRBIS-3" software [29], followed by automated adjustment of the optical parameters for both the objects and the surrounding environment. Subsequently, image scaling and rotation were carried out using a custom Python 3.10-based program, enabling the use of the data for the reconstruction of heat fluxes through the solution of the heat conduction equation [30].

3. Experimental study

3.1. Insulated objects in steady-state air flow.

The study was conducted using a blowdown-type wind tunnel at the Institute of Mechanics, Moscow State University. Its working section consists of a rectangular channel with cross-sectional dimensions of 250 × 174 mm. The axial length of the subsonic nozzle is 690 mm, and the axial distance from the nozzle entrance to the investigated cylinders is 1575 mm (Figure 1).

Air is supplied to the setup's plenum chamber from gasholders which are filled with dried atmospheric air compressed up to 7 atm. In the plenum, the air is "settled" by passing through a honeycomb structure (deturbulizing screen). The Mach number in the working section is controlled by adjusting the air pressure in the plenum. The Reynolds and Mach numbers could not be varied independently. The Mach number of the flow approaching the cylinders ranges from M = 0.35 to 0.60. The upper limit of the Mach number corresponds to the choking condition of the aerodynamic setup. After passing through the working section, the air enters the diffuser and subsequently flowed into the atmosphere.

The objects investigated in the gas flow are thermally insulated cylinders with a diameter of 20 mm, made from Plexiglas, a material with low thermal conductivity of approximately 0.16 W/m·K. The cylinders are positioned 885 mm downstream of the nozzle exit and extend across the full height of the channel. The plane passing through the axes of the cylinders is oriented perpendicular to the direction of the incoming flow velocity. During the experiments, the temperature field around the rear critical line of the cylinders is measured. The difference between the adiabatic wall temperature and the stagnation temperature of the incoming flow is maximal in this region. One of the objectives of the experimental study was to establish the correlation between the adiabatic wall temperature near the rear critical line of the cylinders, the Mach number of the incoming flow, and the relative spacing between the cylinders [31].

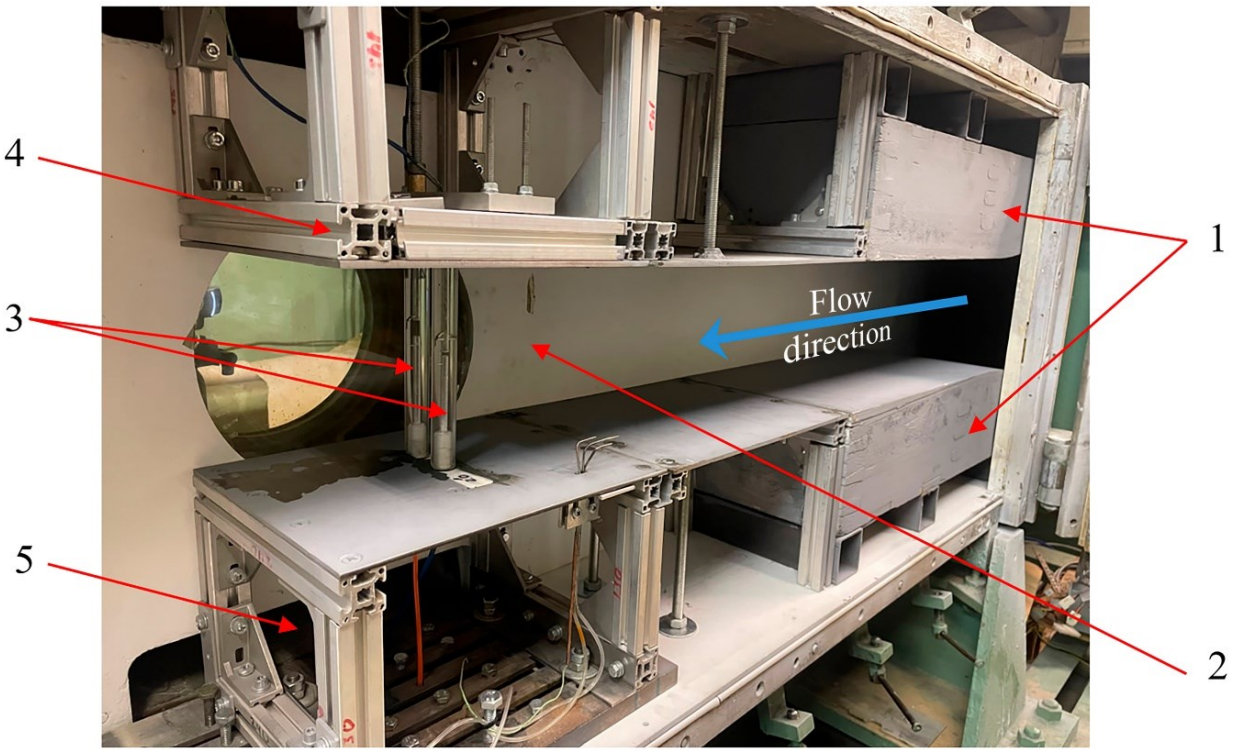

Figure 1. General view of experimental setup 1 (from the IR-camera side): 1 - profiled nozzle's walls, 2 - working channel, 3 - investigated circular cylinders, 4-5 - cylinder mounts within the wind tunnel.

The experimental procedure is carried out as follows. The Mach number in the working section is decreased from values corresponding to the choking regime (M = 0.6) down to M = 0.35. The rate of Mach number variation within the working channel is minimal, measured at 5.5×10^{-4} Mach/s over the Mach number range of 0.6–0.45. This variation occurred due to the discharge rate of the gasholders exceeding their filling rate supplies by a compressor. At lower Mach numbers, specifically within the range of 0.45–0.35, the compressed air flow rate remains nearly constant. The transition between Mach numbers within this range is achieved through external regulation of the plenum pressure. Throughout the entire range of Mach number variation, the stagnation temperature of the incoming flow varies by no more than two degrees. The time interval required to achieve steady-state temperature conditions is about 5 seconds (Figure 2a), during which the Mach number decreases by 0.0055. Thermographic recordings are conducted continuously at a frequency of 0.2 Hz. During data processing, the measurement data are mapped onto the cylindrical surface of the investigated objects for further analysis (Figure 2b).

Based on the obtained dependence of $T_{aw}(M)$, the correlation between the recovery factor (1) and the Mach number of the incoming flow is determined as part of the aerodynamic cooling effect analysis [31]. The recorded surface temperature field not only allows the investigation of the recovery factor distribution around the cylinder's circumference but also facilitates the examination of its non-uniformity along the cylinder's axis, which results from interaction with the boundary layer formed on the channel walls.

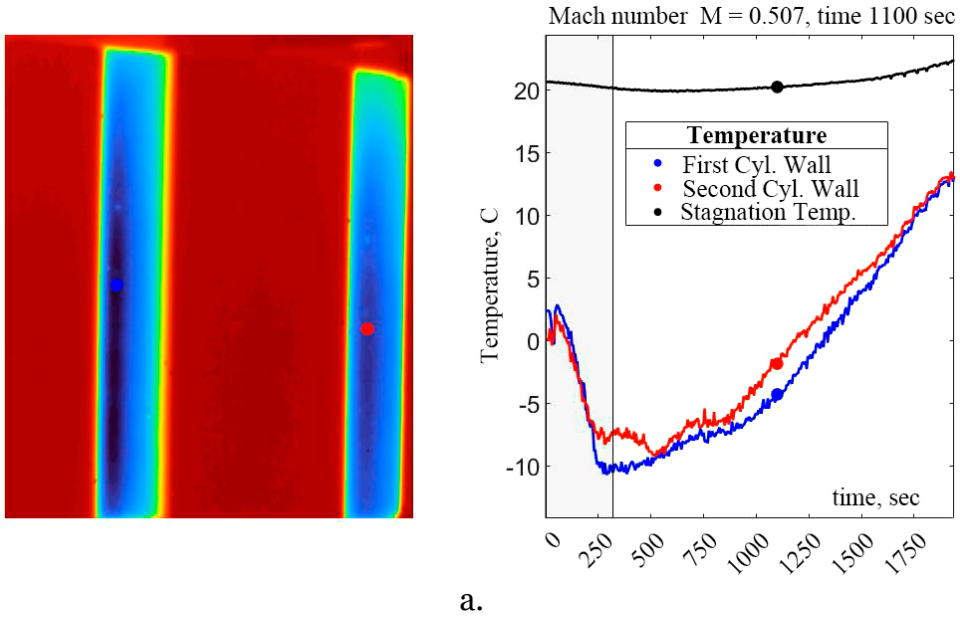

a.

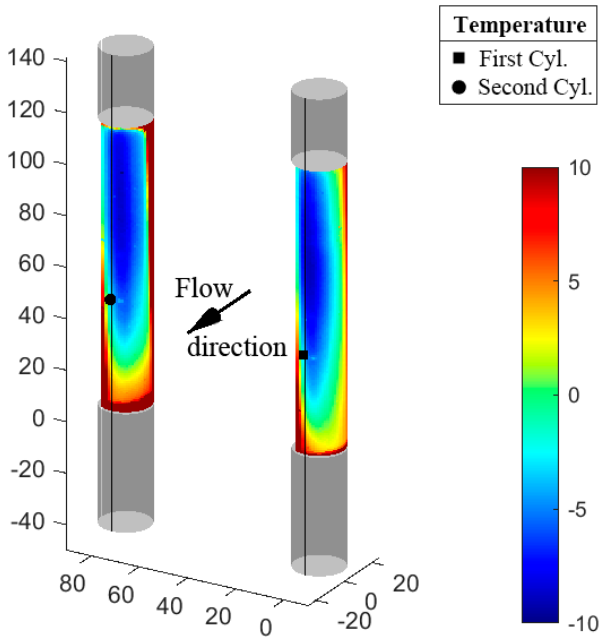

b.

Figure 2. Surface temperatures of thermally insulated objects: a) dependence of adiabatic wall temperature on the Mach number near the rear critical line, b) adiabatic wall temperature of the cylinder.

3.2. The wall cooled by a stationary supersonic flow

Experimental investigations were conducted using a small-size aerodynamic setup (Figure 3) [32].

Compressed air enters the plenum chamber (2), where the flow is equalized within a honeycomb structure. Pressure (3) and stagnation temperature (4) are recorded in the plenum chamber. Following the plenum (and sixfold compression), a shutter (5) is installed to direct the airflow either into the channel or directly into the atmosphere. After further compression in the diffuser (by a factor of 4.2), the air enters the experimental slot channel (6). The calculated Mach number at the exit of the supersonic nozzle is M = 2.0.

The channel's lower and upper walls are flat, with the lower wall heated and the upper wall designed to be replaceable. Heating is achieved by circulating heated liquid coolant along the rear surface of the lower wall. The upper wall features a Zn-Se window (7), transparent in the

infrared range, enabling the registration of the temperature field. The window spans a section of the channel from 0.05 to 0.26 meters.

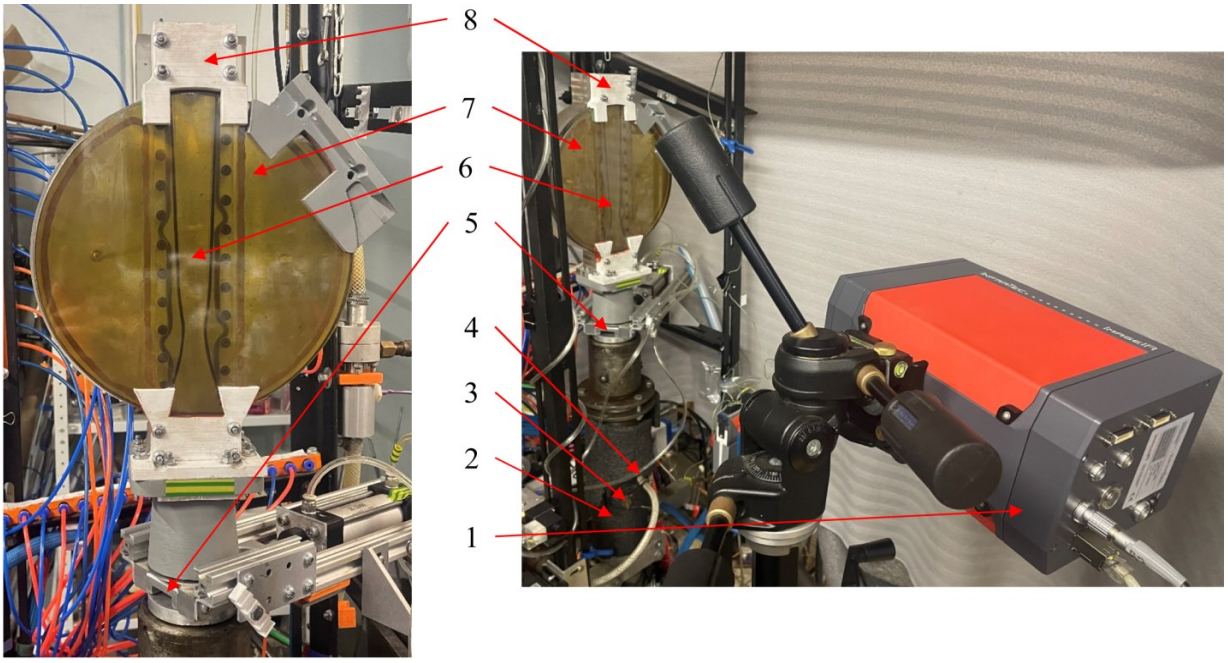

Figure 3. Experimental setup: 1 – IR-camera, 2 - plenum chamber, 3, 4 - temperature and pressure sensors, 5 - shutter, 6 - investigated channel, 7 - upper wall and Zn-Se window, 8 - diffuser.

In the presence of heat transfer with adjacent components and the surrounding environment, it is not possible to directly determine the adiabatic wall temperature. In such cases, methods for recovering boundary conditions and extrapolating the wall temperature to its adiabatic value can be employed. However, these methods are highly sensitive to the accuracy of data transfer to the computational model.

As part of the investigation, an application program was developed for the semi-automatic scaling and rotation of raw thermograms to transfer the data contained within them as boundary conditions for the heat conduction problem onto a finite element mesh. The program was developed using the integrated development environment PyCharm. The primary libraries for data processing are: NumPy, which supports multidimensional arrays and matrices; Matplotlib, used for creating and extracting information from graphical objects; and SciPy, employed for interpolating the obtained thermograms onto the computational mesh for further analysis.

The experimental setup, which involves the preliminary heating of the channel, due to the different thermal conductivities of the mounting components and channel walls, enables clear identification of these objects in the thermogram (Figure 4a). Consequently, the isotherms of the mounting elements, spaced 20 mm apart along the channel length and 45 mm apart across its width, can be used as reference objects for the position and transformation of raw thermograms to further proceeding and analysis. The developed program provides the option to sequentially select a defined area surrounding the objects of interest (the mounting element—four such elements are sufficient for image positioning). Subsequently, for the newly opened window displaying the temperature field, data regarding the isolines (elements of matplotlib.collections) are extracted as objects consisting of a set of points using the **get_paths()** method. For the smoothest isolines, which form concentric circles, the center is determined, ultimately defining the position of the mounting element in the thermogram. After processing several elements, the rotation angle (of the channel/camera) and the scale factors along the channel's length and width can be determined. Since the position of the object

in the frame remains fixed during video recording, the obtained parameters are applied to all recorded thermograms.

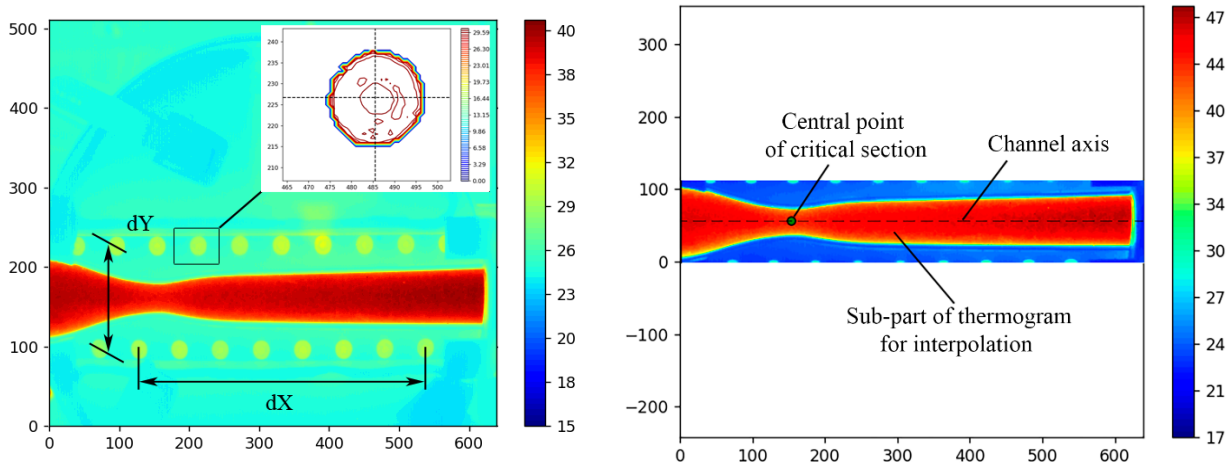

a. b.

Figure 4. Thermogram processing procedure: a) Scaling of the image based on isotherms of reference objects, b) final thermogram for interpolation onto the finite element mesh.

The data from the corrected thermograms are subsequently interpolated onto the finite element model, with the element size chosen to align with the spatial resolution of the IR camera (Figure 5). The interpolation was carried out using Python's built-in functionality (SciPy library), employing Delaunay triangulation.

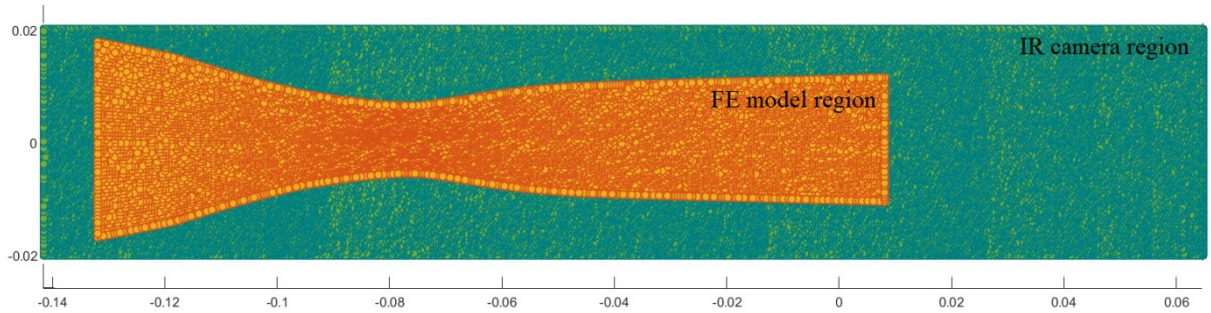

Figure 5. Interpolation of thermogram data onto the FEM model of the channel wall

The experimental wall temperature field of the channel, along with the corresponding calculated heat flux and adiabatic wall temperature, is shown in Figure 6.

Upon the opening of the shutter (5 – Figure 3), the nozzle chokes, and the shock wave begins to shift towards the channel exit. This process can be observed both from the changes in wall temperature, as obtained from the thermograms, and from the reconstructed heat fluxes (Figure 6a).

The increase in the adiabatic wall temperature at a distance of 75 mm from the critical section for the specific steady-flow regime enables the identification of the shock wave's position (Figure 6b). Simultaneously, both the wall temperature and the heat flux continue to decrease over time within the steady flow regime.

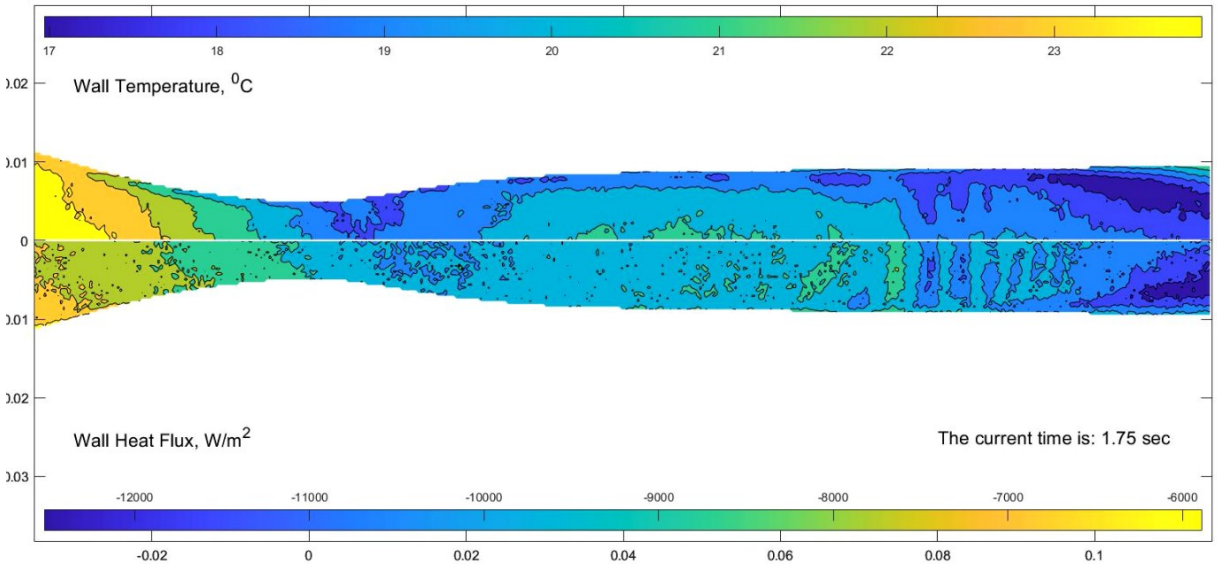

a.

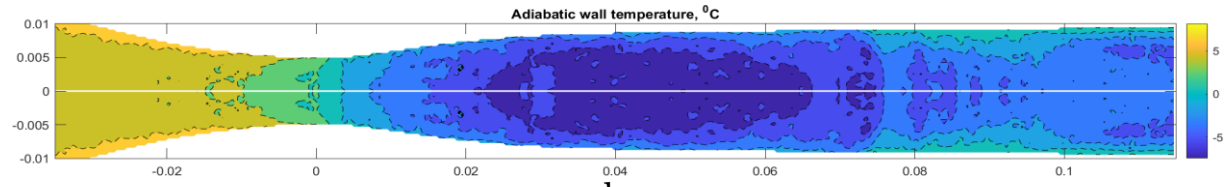

b.

Figure 6. Values at the channel wall: a) change in surface temperature and heat flux during the experiment, b) adiabatic wall temperature of the channel surface for steady state flow condition.

The distribution of adiabatic wall temperature along the channel length can be described as follows: during flow acceleration in the nozzle, the temperature decreases from +10°C to +2°C at the critical section, and then further drops to -5°C in the supersonic section of the nozzle. In the supersonic flow region downstream of the nozzle, the temperature ranges from -5°C and -1°C. Following the shock wave and further downstream, partial recovery occurs, with the temperature rising to +2°C.

4. Conclusion

The potential of non-contact thermographic imaging for investigating heat transfer parameters between the bodies and a high-speed gas flow is demonstrated. An applied software tool for processing sequences of thermograms has been developed, automating the handling of large experimental data sets.

Two methods for measuring adiabatic wall temperature are presented. The first method enables direct measurement of the adiabatic wall temperature during the experiment and does not require an initial temperature difference between the surface under study and the gas flow. The second method involves processing a sequence of thermograms that capture the cooling/heating of the surface. This approach requires an initial temperature difference but significantly reduces the duration of the experiment for determining the adiabatic wall temperature. Additionally, it allows the determination of heat flux values and heat transfer coefficients for steady-state flow parameters.

Moreover, the methods described for determining the adiabatic wall temperature enable the investigation of how flow parameters and surface topology influence the distribution of the temperature recovery coefficient. These methods also allow the precise evaluation of the efficiency of physical processes associated with non-mechanical energy separation.

Acknowledgments

The study was supported by a Russian Science Foundation (project no. 24-79-10035), https://rscf.ru/project/24-79-10035/.

Conflict of interest

The authors of this work declare that they have no conflicts of interest.

References

1. Escudier M.P., Abdel-Hameed A., Johnson M.W., Sutcliffe C.J. Laminarisation and re-transition of a turbulent boundary layer subjected to favourable pressure gradient // Exp. Fluids. 1998. Vol. 25, № 5–6. P. 491–502.
2. Mee D.J., Chiu H.S., Ireland P.T. Techniques for detailed heat transfer measurements in cold supersonic blowdown tunnels using thermochromic liquid crystals // Int. J. Heat Mass Transf. 2002. Vol. 45, № 16. P. 3287–3297.
3. Kiselev N.A., Malastowski N.S., Vinogradov Y.A., Zditovets A.G. Experimental and numerical study of heat transfer under laminarization condition in a small size supersonic nozzle // Int. J. Therm. Sci. 2023. Vol. 187. P. 108182.
4. Bartkus G. V., Kuznetsov V. V. Experimental Study of Gas-Liquid Flow Patterns in Slit Channel with Cross-Junction Mixer // J. Eng. Thermophys. 2021. Vol. 30, № 1. P. 14–18.
5. Vavilov S.N., Vasil'ev N. V., Zeigarnik Y.A. Vapor Explosion: Experimental Observations // Therm. Eng. 2022. Vol. 69, № 1. P. 66–71.
6. Vasil'ev N.V., Vavilov S.N., Zeigarnik Y.A., Lidzhiev E.A. Visualization of the Structure of Vapor-Liquid Flow During Subcooled R113 Refrigerant Boiling Under Preburnout Conditions // Sci. Vis. 2024. Vol. 16, № 3. P. 79–86.
7. Doroshchenko I.A., Znamenskaya I.A., Sysoev N.N., Lutsky A.E. High-speed Flow Structures Detection and Tracking in Multiple Shadow Images with Matching to CFD using Convolutional Neural Networks // Sci. Vis. 2022. Vol. 14, № 4.
8. Boiko A.V., Ivanov A.V., Borodulin V.I., Mischenko D.A. Quantification technique of transition to turbulence in boundary layers using infrared thermography // Int. J. Heat Mass Transf. 2022. Vol. 183. P. 122065.
9. Alifanov, O. M., Budnik, S. A., Nenarokomov, A. V., Salosina, M. O. (2023). Study of the Thermophysical Properties of Promising Thermal Insulation Materials for Space Engineering. High Temperature, 61(4), 517–524. https://doi.org/10.1134/S0018151X23040016
10. Kiselev N.A., Malastowski N.S., Zditovets A.G., Vinogradov Y.A. Reynolds analogy violation for a compressible turbulent boundary layer with pressure gradient in a small-size supersonic slot channel // Int. J. Therm. Sci. Elsevier Masson SAS, 2024. Vol. 200, № November 2023. P. 108973.
11. Devyatkov V. V., Alfimtsev A.N., Taranyan A.R. Multicamera Human Re-Identification based on Covariance Descriptor // Pattern Recognit. Image Anal. 2018. Vol. 28, № 2. P. 232–242.
12. Pohlhausen E. Der Wärmeaustausch zwischen festen Körpern und Flüssigkeiten mit kleiner reibung und kleiner Wärmeleitung // ZAMM - Zeitschrift für Angew. Math. und Mech. 1921. Vol. 1, № 2. P. 115–121.
13. Johnson H.., Rubesin M.W. Aerodynamic heating and convective heat transfer - Summary of literature survey // Trans. ASME. 1949. Vol. 71, № 5. P. 447–456.
14. Leontiev, A. I., Lushchik, V. G., Makarova, M. S., Popovich, S. S. (2022). Temperature Recovery Factor in a Compressible Turbulent Boundary Layer. High Temperature, 60(3), 409–431. https://doi.org/10.1134/S0018151X22030117
15. Hurst C., Schulz A., Wittig S. Comparison of calculated and measured heat transfer coeffiecients for transonic and supersonic boundary-layer flows // Proc. ASME Turbo Expo. 1994. Vol. 4, № April 1995. P. 248–254.

16. Nash-Webber J.L., Oates G.C. An Engineering Approach to the Design of Laminarizing Nozzle Flows // J. Basic Eng. 1972. Vol. 94, № 4. P. 897–903.
17. Schoenman L., Block P. Laminar boundary-layer heat transfer in low-thrust rocket nozzles // J. Spacecr. Rockets. 1968. Vol. 5, № 9. P. 1082–1089.
18. Stoll J., Straub J. Film cooling and heat transfer in nozzles // J. Turbomach. 1988. Vol. 110, № 1. P. 57–65.
19. Mutama K.R., Iacovides H. The Investigation of developing flow and heat transfer in a long converging duct // J. Heat Transfer. 1993. Vol. 115, № 4. P. 897–903.
20. Back L.H., Cuffel R.F. Turbulent Boundary Layer and Heat Transfer Measurements Along a Convergent-Divergent Nozzle // J. Heat Transfer. 1971. Vol. 93, № 4. P. 397.
21. Back L.H., Massier P.F., Gier H.L. Convective heat transfer in a convergent-divergent nozzle // Int. J. Heat Mass Transf. 1964. Vol. 7, № 5. P. 549–568.
22. Back L.H., Cuffel R.F., Massier P.F. Laminarization of a Turbulent Boundary Layer in Nozzle Flow—Boundary Layer and Heat Transfer Measurements With Wall Cooling // J. Heat Transfer. 1970. Vol. 92, № 3. P. 333–344.
23. Leontiev A.I., Zditovets A.G., Kiselev N.A., Vinogradov Y.A., Strongin M.M. Experimental investigation of energy (temperature) separation of a high-velocity air flow in a cylindrical channel with a permeable wall // Exp. Therm. Fluid Sci. 2019. Vol. 105. P. 206–215.
24. Rubesin M.W. A modified Reynolds analogy for the compressible turbulent boundary layer on a flat plate // NACA TN 2917.
25. Modenini D., Schrijer F.F.J. Heat transfer measurements in a supersonic wind tunnel through inverse temperature data reduction: Application to a backward facing step // Quant. Infrared Thermogr. J. 2012. Vol. 9, № 2. P. 209–230.
26. Avallone F., Greco C.S., Schrijer F.F.J., Cardone G. A low-computational-cost inverse heat transfer technique for convective heat transfer measurements in hypersonic flows // Exp. Fluids. Springer Berlin Heidelberg, 2015. Vol. 56, № 4.
27. Sousa J.F.L., Lavagnoli S., Paniagua G., Villafañe L. Three-dimensional (3D) inverse heat flux evaluation based on infrared thermography // Quant. Infrared Thermogr. J. 2012. Vol. 9, № 2. P. 177–191.
28. Sousa J., Villafañe L., Paniagua G. Thermal analysis and modeling of surface heat exchangers operating in the transonic regime // Energy. 2014. Vol. 64, № January. P. 961–969.
29. Thermography software IRBIS® 3 active , 2025. Accessed: February 16th, 2025. [Online]. Available: https://www.infratec.eu/thermography/thermographic-software/irbis3-active/.
30. Kiselev N.A., Malastovskii N.S., Zditovets A.G., Vinogradov Y.A. Experimental Study of the Heat Transfer at Compressible Gas Flow with a Favorable Pressure Gradient // High Temp. 2023. Vol. 61, № 4. P. 535–543.
31. Zditovets A.G., Kiselev N.A., Popovich S.S., Vinogradov Y.A. Experimental investigation of the Eckert-Weise effect (aerodynamic cooling) of pair side-by-side circular cylinders in a compressible cross-flow // Int. J. Heat Mass Transf. 2024. Vol. 233. P. 126061.
32. Zditovets A.G., Kiselev N., Vinogradov Y.A., Popovich S. Adiabatic wall temperature in the supersonic flow of moist air with spontaneous condensation // Exp. Therm. Fluid Sci. 2024. Vol. 150. P. 111057.